Analytical Investigation of GaAs and Si Characteristics: Impact of Temperature and Doping Concentration

Monasipova Renata Fidanovna[1], Khakimova Yakutkhon[2], Eshkobilov Olim Kholikulovich[3], Aliyarova Lola Abdijabborovna[3].

[1]Gulistan State University, Gulistan, Uzbekistan
[2]Tashkent state Transport University, Tashkent, Uzbekistan
[3]Karshi State Technical University, Karshi, Uzbekistan

Abstract

In this study, we analytically investigate the electrophysical characteristics of the p-Si/n-GaAs heterojunction (HJ) over a temperature range of 50 K to 500 K, with 50 K increments, while considering different doping concentrations. Our analysis focuses on band gap narrowing (BGN), temperature-dependent variations in the band gap of GaAs and Si, and the built-in potential as a function of temperature. Specifically, we examine a p-n junction structure with a p-Si region of 45 μm and an n-GaAs of 100 μm. Our findings indicate that the depletion region thickness in the p-Si/n-GaAs HJ increases with rising temperature. At 300 K, the band gap difference between GaAs and Si is found to be 0.31 eV, which aligns well with experimental data. Additionally, at 300 K, we calculate a conduction band offset (ΔE_C) of 0.04 eV and a valence band offset (ΔE_V) of 0.27 eV. When the doping concentration varies from 2e15 to 2e18, BGN decreases by 2 meV. Furthermore, as temperature increases, the built-in potential of the p-Si/n-GaAs HJ decreases by 76 mV.

Keywords: *heterojunction (HJ), conduction band offset, absorbing, built-in potential, band gap narrowing (BGN)*

1. Introduction

The rapid advancements in semiconductor electronics research have significantly improved the design, optimization, and functionality of modern devices. Breakthroughs such as two-dimensional transistors [1-4], nanowires, and, most notably, radial p-n junction structures have expanded the possibilities for nanoscale applications [5-9]. Among these innovations, radial p-n junctions offer distinct advantages over conventional planar designs, particularly in submicron nanowires. Over the past two decades, these structures have attracted increasing attention due to their enhanced optical and electronic properties, making them ideal for applications in photodiodes, optical sensors, thermal detectors, photovoltaic detectors, and solar cells [10-14].

By optimizing light absorption and carrier collection[15-18], radial p-n junctions effectively minimize optical losses, leading to improved energy conversion efficiency. Their perpendicular alignment for light absorption and carrier transport further enables high-frequency applications, including high-speed electronics and wireless communication [19]. Additionally, these structures play a crucial role in high-performance photodetectors, avalanche photodiodes, photovoltaic devices, gamma-ray detectors, and infrared sensors, where their architecture provides exceptional efficiency, speed, and sensitivity key factors for advanced semiconductor applications [20].

Given their wide-ranging applications, a comprehensive study of the electrophysical properties of these junctions, particularly ionization processes and temperature-dependent performance, is essential. Both theoretical modeling and experimental validation are required to ensure the reliability and precision of these devices. While p-n junctions have been extensively investigated, heterojunction structures remain less explored. Despite the emergence of new semiconductor materials, GaAs remains a dominant choice for optoelectronic devices, whereas Si continues to be widely used due to its well-established technological infrastructure and natural abundance.

From this perspective, the p-Si/n-GaAs (HJ) has been selected for this study. This work aims to bridge the existing research gap by analyzing the electrophysical properties of the p-Si/n-GaAs HJ using theoretical and analytical approaches. Through mathematical modeling, we examine the behavior of the p-Si/n-GaAs RHJ under varying temperatures and applied voltages, providing valuable insights into its performance characteristics and potential future applications. Si nanowires (SiNWs) have been extensively studied due to their compatibility with existing silicon-based semiconductor technology. They show excellent electronic properties when scaled down to the nanometer range. Applications: SiNWs are used in sensors, transistors, and solar cells, leveraging their high surface-to-volume ratio for better performance in miniaturized electronic devices [21]. Challenges: SiNWs often face issues with carrier mobility and surface recombination, especially under high doping levels.

GaAs nanowires (GaAsNWs) offer superior electron mobility and optical properties compared to Si, making them ideal for high-speed electronics and optoelectronics [22]. Their direct bandgap also makes them ideal for light-emitting applications. Applications: GaAsNWs are used in photodetectors, LEDs, and solar cells due to their efficient light absorption and emission characteristics. Advantages: GaAs nanowires outperform Si nanowires in terms of speed and efficiency for optical and high-frequency applications due to their material properties [23].

Comparison: GaAsNWs generally outperform SiNWs in high-frequency, optoelectronic, and photonic applications due to their higher mobility and direct bandgap. Scalability: SiNWs are more easily integrated into conventional CMOS processes, while GaAsNWs, though more efficient, may require more specialized

fabrication techniques. GaAs nanowires are more suitable for optical and high-speed applications [24], while Si nanowires continue to be an important material in conventional electronic and scalable technologies. The properties of Silicon (Si) and Gallium Arsenide (GaAs) semiconductors are significantly influenced by temperature and doping concentration. As temperature increases, both materials experience a decrease in carrier mobility and a reduction in bandgap, with GaAs having a smaller temperature coefficient. Doping concentration increases carrier concentration and conductivity, but also reduces mobility due to impurity scattering. Higher doping leads to a narrower depletion region in p-n junctions, and while GaAs offers higher electron mobility, it is more sensitive to high doping levels, potentially leading to performance degradation. Si, on the other hand, is more stable in terms of doping-induced effects.

2. Materials

"In this study, we have selected a core of p-Si with a radius of 45 μm and a shell of n-GaAs with a radius of 100 μm as the object of interest. Based on the operating temperatures of semiconductor devices made from Si and GaAs, the temperature range was chosen to be between 50 K and 500 K, with increments of 50 K. The interval $d_{p-n} = r_p < r < r_n$ represents the depletion region and this depends on temperature and external voltage and is represented by the expression (1):

$$d_{p-n} = \sqrt{\frac{2(\varepsilon_{GaAs} N_A + \varepsilon_{Si} N_D)(\varphi_{bi}(T) - U)}{q\varepsilon_{Si}\varepsilon_{GaAs}\varepsilon_0 N_A \cdot N_D}} \quad (1)$$

where, $\varepsilon_{Si}, \varepsilon_{GaAs}$ are and dielectric constant of the Si and GaAs respectively, $\varepsilon_0 = 8.85 \cdot 10^{-12}\ F \cdot m^{-1}$ electrical constant. Many studies have conducted theoretical work without considering the dependence of effective mass on temperature and electric field. To address this gap, we calculated the temperature-dependent effective mass of electrons and holes using equation (2).

$$m^*_{(n,p)} = m(T_0) \cdot \left(1 + \beta_{(n,p)} \cdot (T - T_0)\right) \quad (2)$$

Where, $m(T_0)$ is mass , $\beta_{(n,p)}$ is the temperature coefficient of the effective mass (which can be determined experimentally or from theoretical models). T_{0GaAs} and T_{0Si} are Debye temperature GaAs and Si respectively.

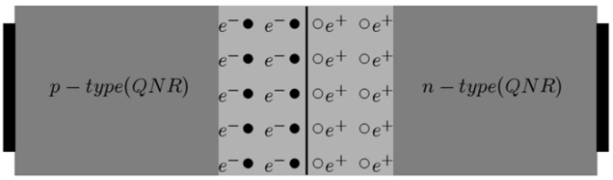

Figure 1. This figure shows a 2D cross-section of the submicron p-n junction structures. The light gray area represents the n-type region, the dark gray area represents the p-type region, and the very light gray area denotes the depletion region

Figure 1 shows the cross-sectional view of the selected p-Si/n-GaAs (RHJ) sample, cut along the Z-axis. Where r denotes the radial dimension, + and − represents the densities of ionized N_D^+ donor and N_A^- acceptor atoms respectively, at the interface of the radial p-n heterojunction within the depletion region. If full ionization case $N_D^+ = N_D$, $N_A^- = N_A$. In Figure 1, the interval $0 < r < r_p$ represents the p-type quasi-neutral region (QNR), the interval $r_p < r < r_n$ represents the depletion region in the radial p-n heterojunction junction, the interval $r_n < r < 2R$ represents the n-type quasi-neutral region (QNR). In heterojunctions, there are differences in the conduction band ΔE_C and valence band ΔE_V at the interface, and these differences change with temperature and concentration. As a result, there is a difference in the band gap between Si and GaAs, as described by expression (3).

$$\Delta E_g(T, n, p) = \Delta E_g(T) - \Delta E_{BGN}(n, p) \quad (3)$$

Where, $\Delta E_g(T)$ is the term that depends on temperature, and $\Delta E_{BGN}(n,p)$ represents band gap narrowing, which is influenced by concentration, as described by expression (4).

$$\Delta E_{BGN}(n, p) = A \cdot \sqrt[3]{N} + B \cdot \sqrt[4]{N} + C \cdot \sqrt{N} + D \cdot \sqrt{N} \quad (4)$$

where A, B, C, and D are material-dependent semi-empirical coefficients [25]; the values for Si and GaAs are provided in Table 1. The influence of temperature and concentration on electron affinity was also examined, as expressed by equation (5).

$$\chi(T, n, p) = \chi_0 - \alpha \cdot (T - T_0) + \lambda \cdot \ln\left(\frac{(n, p)}{N_{eff}}\right) \quad (5)$$

The energy levels ΔE_C and ΔE_V are influenced by temperature. For instance, as temperature increases, the band gap can change, affecting the thermal generation of charge carriers and the performance of devices like diodes and transistors.

$$\Delta E_V(T) = \Delta E_V(0) + T \cdot \left(\gamma_{GaAs} - \gamma_{Si}\right) \quad (6a)$$

$$\Delta E_C(T) = \Delta E_V(T) + \Delta E_g(T) \quad (6b)$$

Here, γ is a coefficient that describes how the valence band shifts with temperature. $\gamma_{GaAs}, \gamma_{Si}$ are -0.006 and -0.001 eV/K respectively. The electrostatic potential difference in the p-Si/n-GaAs radial heterojunction varies with the applied external voltage and can be expressed as follows (7):

$$\varphi_{bi}(T) = \Delta E_g(T) - \frac{kT}{q} \cdot \ln\left(\frac{N_A \cdot N_D}{n_{iGaAs} \cdot n_{iSi}}\right) \quad (7)$$

In this context, k represents the Boltzmann constant, T is the absolute temperature in Kelvin, and q denotes the elementary charge of an electron. The symbols N_A and N_D correspond to the concentrations of acceptor and donor impurities, respectively, while n_i^{Si} and n_i^{GaAs} signify the intrinsic carrier concentrations of Silicon and Gallium Arsenide. The calculations based on these equations and

material parameters are presented in the *Results and Discussion* section, where the findings are evaluated against initial predictions.

Table 1. Coefficients A, B, C, D for Si and GaAs materials

Symbol	Si		GaAs		Unit
A	n-type	p-type	n-type	p-type	eVcm
	$1.02 \cdot 10^{-8}$	$1.11 \cdot 10^{-8}$	$1.65 \cdot 10^{-8}$	$9.77 \cdot 10^{-9}$	
B	$4.15 \cdot 10^{-7}$	$4.79 \cdot 10^{-7}$	$2.38 \cdot 10^{-7}$	$3.87 \cdot 10^{-7}$	$eVcm^{3/4}$
C	$1.45 \cdot 10^{-12}$	$3.23 \cdot 10^{-12}$	$1.83 \cdot 10^{-11}$	$3.41 \cdot 10^{-12}$	$eVcm^{3/2}$
D	$1.48 \cdot 10^{-12}$	$1.81 \cdot 10^{-12}$	$7.25 \cdot 10^{-11}$	$4.84 \cdot 10^{-13}$	$eVcm^{3/2}$

3. Discussion

The effective mass plays a crucial role in governing the movement of electrons and holes within a crystal. Since it varies with temperature, it directly impacts their behavior. Figure 2 depicts the variation in the effective mass of electrons and holes in Si and GaAs materials.

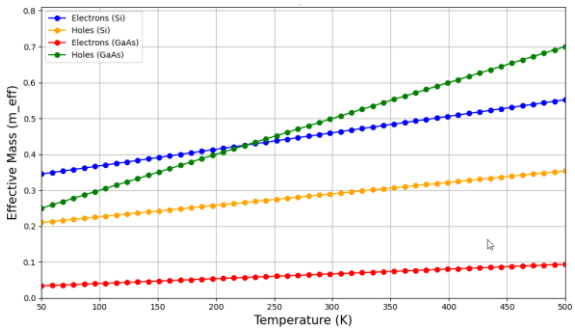

Figure 2. Temperature-dependent effective mass of electrons and holes in Si and GaAs.

The plot illustrates the temperature dependence of the effective masses of electrons and holes in silicon (Si) and gallium arsenide (GaAs) over a range of 50 K to 500 K. In both materials, the effective mass of charge carriers increases slightly with temperature. In Si, the electron effective mass starts at approximately $0.46m_e$, while the hole effective mass begins at $0.29m_e$, both exhibiting a gradual increase. For GaAs, electrons have a significantly lower effective mass, starting around $0.067m_e$, whereas holes begin at $0.5m_e$ and show a more pronounced increase as temperature rises.

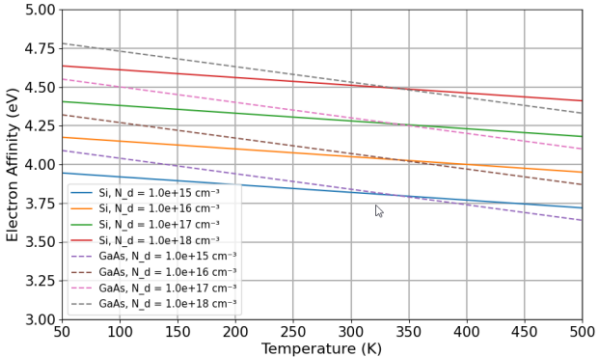

Figure 3. Electron affinity of p-Si and n-GaAs as a function of temperature.

Figure 3 demonstrates that the electron affinity of both Si and GaAs decreases with varying doping concentrations across a temperature range of 50 K to 500 K. Up to 350 K, GaAs exhibits a higher electron affinity than Si, but beyond this temperature, its electron affinity becomes lower. Understanding the dependence of electron affinity on temperature and doping concentration is crucial for optimizing band alignment, carrier transport, and device stability in semiconductor applications. This knowledge facilitates the precise design of heterojunctions, doping profiles, and material selection, ultimately enhancing the performance and reliability of devices such as transistors, solar cells, and optoelectronic components. These trends are influenced by material-specific properties, particularly the significant mass disparity between electrons and holes in GaAs, which benefits high-mobility and optoelectronic applications. Recognizing these variations is essential for optimizing the performance of electronic and optical devices across different temperature ranges.

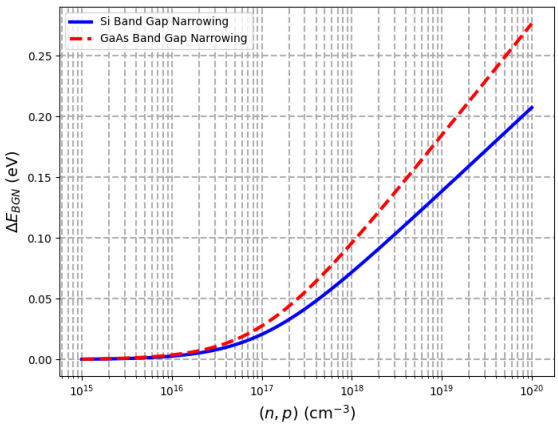

Figure 4. Band gap narrowing in Si and GaAs as a function of temperature.

Figure 4 illustrates the conduction and valence band energies as functions of temperature for Si ($\Delta E_{BGN}Si(p)$ and GaAs ($\Delta E_{BGN}GaAs(n)$.The blue curve represents ($\Delta E_{BGN}Si(p)$ and ($\Delta E_{BGN}GaAs(n)$, which increases from approximately 10^{15} to 10^{20} cm^{-3} as the hole concentration (p) rises. Similarly, the red dashed line represents $\Delta E_{BGN}GaAs(n)$, exhibiting a comparable upward trend with

increasing electron concentration (n). This comparison highlights the distinct energy band characteristics of Si and GaAs over a wide range of carrier concentrations, providing crucial insights into their performance in semiconductor applications.

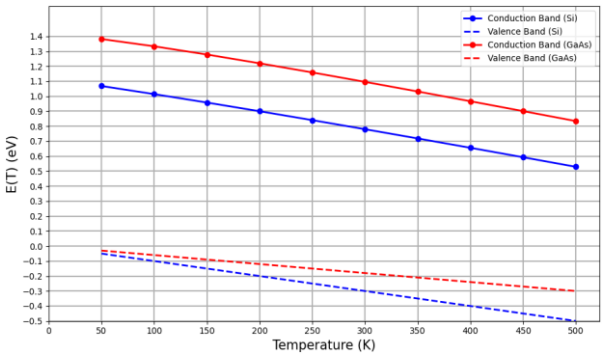

Figure 5. Conduction and valence band energies of Si and GaAs as a function of temperature.

Figure 5 illustrates the temperature dependence of the conduction and valence band energies in Si and GaAs over a range from 50 K to 500 K, showing a decrease in both energy levels as temperature increases. These changes significantly affect electronic properties, including band alignment and carrier dynamics. Understanding these variations is crucial for designing temperature-sensitive semiconductor devices, such as diodes, transistors, and heterojunctions, to ensure optimal performance across a wide temperature range. The conduction and valence band energies in both silicon and gallium arsenide exhibit distinct temperature dependence, which is essential for the effective design and optimization of semiconductor devices.

Figure 6 shows that the band gap and built-in potential of Si and GaAs decrease with rising temperature, with GaAs experiencing a steeper decline in the band gap. These temperature-dependent changes, influenced by material-specific properties, play a significant role in the behavior of semiconductor devices. These trends highlight the importance of considering temperature effects in semiconductor device design. As both the band gap and built-in potential decrease, it is essential for engineers to optimize device performance, particularly in power electronics and optoelectronics, where thermal stability is crucial.

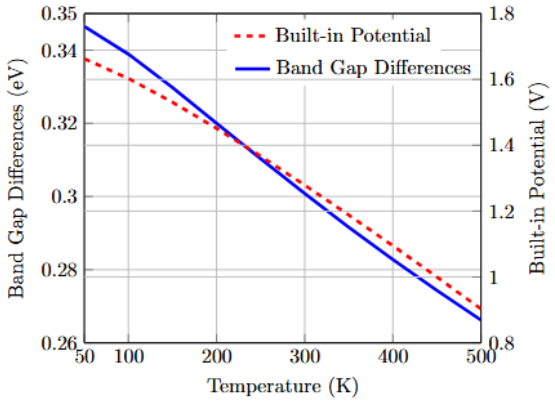

Figure 6. Differences of Band Gap and Built-in Potential as a function of Temperature

Figure 6 illustrates the relationship between the band gap and built-in potential as a function of temperature, emphasizing their crucial role in shaping the electrical behavior of semiconductor devices. Understanding these dependencies is essential for optimizing temperature-sensitive components such as p-n junctions, LEDs, and solar cells.

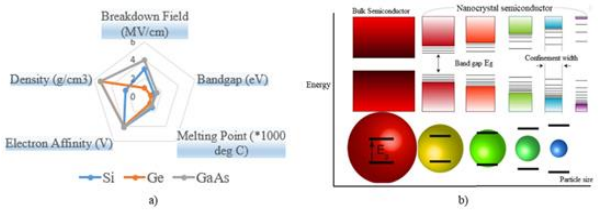

Figure 7. a) Comparison of the features of semiconductor materials, b) Bandgap dependence on quantum size confinement.

In figure **7,** a) Si High breakdown field & melting point, ideal for power devices. Ge Lowest bandgap, high carrier mobility but thermally sensitive. GaAs: Larger bandgap, excellent for optoelectronics, b) Quantum Confinement: Smaller nanocrystals → Wider bandgap. Key for tunable properties in quantum dots, LEDs, and photodetectors.

Our model predicts a band gap difference of 0.31 eV between GaAs and Si at 300 K, aligning well with experimental observations. At this temperature, the conduction band offset (ΔEC) is calculated as 0.04 eV, while the valence band offset (ΔEV) is 0.27 eV. The plot demonstrates how temperature influences two key semiconductor properties: band gap differences and built-in potential. As temperature increases from 50 K to 500 K, both parameters decline. Specifically, the band gap narrows from approximately 0.35 eV to 0.26 eV due to enhanced lattice vibrations and thermal excitation, which lower the energy required for electron transitions. This narrowing can elevate intrinsic carrier concentrations, improving conductivity but also potentially leading to undesirable leakage currents in high-temperature applications. The built-in potential decreases from approximately 1.66 V to 0.9 V, indicating a weakening of the internal electric field. This decline suggests that thermal effects play a significant role in charge carrier dynamics, potentially reducing the efficiency of devices that rely on strong potential barriers, such as diodes and transistors, in high-temperature environments.

This analysis underscores the need for further research into the underlying mechanisms of these temperature effects and their impact on specific device architectures. Figure 7 illustrates the temperature-dependent variation of the band gap in silicon (Si) and gallium arsenide (GaAs) from 40 K to 500 K. GaAs initially exhibits a higher band gap of 1.52 eV at 40 K, which decreases to about 1.35 eV at 500 K, demonstrating greater thermal sensitivity compared to Si. While this temperature dependence can influence GaAs's performance at high temperatures, its direct band gap remains advantageous for optoelectronic applications, particularly in LEDs and laser diodes.

Overall, a deeper understanding of these thermal properties is essential for designing reliable semiconductor devices, whether prioritizing Si's thermal

stability or leveraging GaAs's superior high-frequency and optical performance.

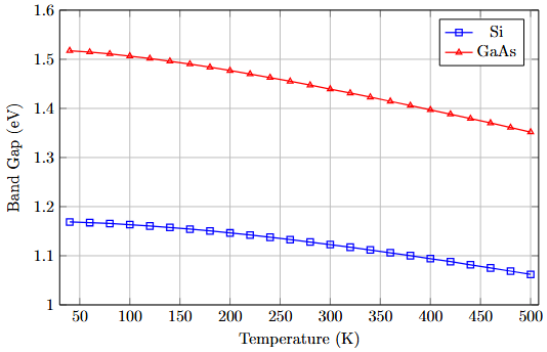

Figure 8. Band gaps of Si and GaAs as a function of temperature

Figure 8 shows that the intrinsic carrier concentration, for Si and GaAs rises exponentially from 50 K to 500 K due to thermal generation of carriers. GaAs, with its narrower band gap, reaches higher $n_i(T)$ values, indicating greater thermal sensitivity compared to Si. Here, majority carrier concentration $p_p = n_n = N_A = N_D = 2 \cdot 10^{16} cm^{-3}$, minority carrier concentration $p_n = n_i^2 / N_D$ and $n_p = n_i^2 / N_A$. Here, $n_i = 1.7 \cdot 10^6 cm^{-3}$ is the intrinsic concentration, for *GaAs*, $n_i = 1.5 \cdot 10^{10} cm^{-3}$ for *Si* at 300 K.

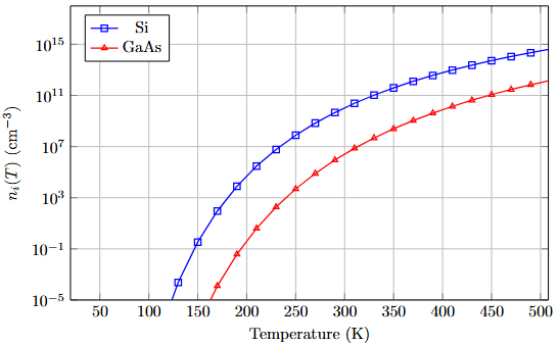

Figure 9. Intrinsic carrier concentration of Si and GaAs as a function of temperature.

The conductivity of these materials is strongly influenced by temperature variations, as higher temperatures can affect device stability. Silicon's high thermal stability makes it ideal for general electronic applications, while GaAs, with its thermal sensitivity and direct band gap, is particularly suited for optoelectronic and high-frequency applications, especially in controlled environments. Understanding these properties is crucial for optimizing device performance across varying temperature conditions. This graph shows the intrinsic carrier concentration $n_i(T)$ of Si and GaAs as a function of temperature. As temperature increases, n_i rises exponentially for both materials, with Si exhibiting a higher nin_ini due to its smaller band gap (1.12 eV vs. 1.42 eV for GaAs at 300 K). This indicates that Si is more affected by thermal excitation, leading to higher leakage currents at elevated temperatures. GaAs, with its lower ni, is better suited for high-frequency and optoelectronic applications, maintaining stability despite band gap narrowing.

3. Conclusion

In conclusion, our analytical study of the p-Si/n-GaAs radial heterojunction, specifically with a core radius of 0.5 μm and a shell radius of 1 μm, provides significant insights into its electrophysical features over a temperature range of 50 K to 500 K. We observed that the thickness of the depletion region increases with rising temperature, reflecting the complex dynamics within the heterojunction. At 300 K, the band gap difference between GaAs and Si was determined to be 0.31 eV, which aligns closely with experimental data, while the conduction band offset was calculated at ΔE_C = 0.04 eV and the valence band offset at ΔE_V = 0.27 eV. Additionally, our analysis showed that band gap narrowing (BGN) decreases by 2 meV as doping concentrations increase from $2 \cdot 10^{15}$ to $2 \cdot 10^{18}$. Moreover, we found that the built-in potential of the p-Si/n-GaAs heterojunction decreases by 76 mV with an increase in temperature. These quantitative findings highlight the importance of considering both the geometric parameters and doping concentration in the design and optimization of radial heterojunctions, providing a solid foundation for future advancements in semiconductor device applications.

Acknowledgments

The authors would like to thank the conference organizers.

References

[1] O.V. Pylypova, A.A. Evtukh, P.V. Parfenyuk, I.I. Ivanov, I.M. Korobchuk, O.O. Havryliuk, and O.Yu. Semchuk, Opto-Electronics Review, **27**(2), 143 (2019). https://doi.org/10.1016/j.opelre.2019.05.003.

[2] R. Ragi, R.V.T. da Nobrega, U.R. Duarte, and M.A. Romero, IEEE Trans. Nanotechnol. **15**(4), 627 (2016). https://doi.org/10.1109/TNANO.2016.2567323.

[3] Abdullayev, J. Sh., Sapaev, I. B. (2024). Оптимизация влияния легирования и температуры на электрофизические характеристики p-n и p-i-n переходных структур. Eurasian Physical Technical Journal, 21(3(49), 21–28. (https://doi.org/10.31489/2024No3/21-28).

[4] Abdullayev, J., & Sapaev, I. B. (2024). Factors Influencing the Ideality Factor of Semiconductor p-n Junction Structures at Cryogenic Temperatures. *East European Journal of Physics*, (4), 329-333. https://doi.org/10.26565/2312-4334-2024-4-37

[5] R.D. Trevisoli, R.T. Doria, M. de Souza, S. Das, I. Ferain, and M.A. Pavanello, IEEE Trans. Electron Devices, **59**(12), 3510 (2012). https://doi.org/10.1109/TED.2012.2219055.

[6] N.D. Akhavan, I. Ferain, P. Razavi, R. Yu, and J.-P. Colinge, Appl. Phys. Lett. **98**(10), 103510 (2011). https://doi.org/10.1063/1.3559625.

[7] A.V. Babichev, H. Zhang, P. Lavenus, F.H. Julien, A.Y. Egorov, Y.T. Lin, and M. Tchernycheva, Applied Physics Letters, **103**(20), 201103 (2013). https://doi.org/10.1063/1.4829756.

[8] R. Elbersen, R.M. Tiggelaar, A. Milbrat, G. Mul, H. Gardeniers, and J. Huskens, Advanced Energy

Materials, 5(6), 1401745 (2014). https://doi.org/10.1002/aenm.201401745.

[9] D.H.K. Murthy, T. Xu, W.H. Chen, A.J. Houtepen, T.J. Savenije, L.D.A. Siebbeles, *et al*., Nanotechnology, **22**(31), 315710 (2011). https://doi.org/10.1088/0957-4484/22/31/315710.

[10] B. Pal, K.J. Sarkar, and P. Banerji, Solar Energy Materials and Solar Cells, **204**, 110217 (2020). https://doi.org/10.1016/j.solmat.2019.110217.

[11] Abdullayev, J. and Sapaev, I. 2024. Modeling and calibration of electrical features of p-n junctions based on Si and GaAs. *Physical Sciences and Technology*. 11, 3-4 (Dec. 2024), 39–48. https://doi.org/10.26577/phst2024v11i2b05.

[12] I. Aberg, G. Vescovi, D. Asoli, U. Naseem, J.P. Gilboy, C. Sundvall, and L. Samuelson, IEEE Journal of Photovoltaics, **6**(1), 185 (2016). https://doi.org/10.1109/JPHOTOV.2015.2484967.

[13] J. Sh. Abdullayev, I. B. Sapaev, Kh. N. Juraev, Theoretical analysis of incomplete ionization on the electrical behavior of radial p-n junction structures // Low Temp. Phys. 51, 60–64 (2025), (https://doi.org/10.1063/10.0034646).

[14] J.Sh. Abdullayev, I.B. Sapaev, Analytic Analysis of the Features of GaAs/Si Radial Heterojunctions: Influence of Temperature and Concentration // East European Journal of Physics, (1), 204-210. (https://doi.org/10.26565/2312-4334-2025-1-21).

[15] J.Sh. Abdullayev, Influence of Linear Doping Profiles on the Electrophysical Features of p-n Junctions // East European Journal of Physics, (1), 245-249. (https://doi.org/10.26565/2312-4334-2025-1-26).

[16] S. C. Jain and D. J. Roulston, “A Simple Expression for Band Gap Narrowing (BGN) in Heavily Doped Si, Ge, GaAs and Ge_xSi_{1-x} Strained Layers,” Solid-State Electronics, vol.34, no. 5, pp. 453–465, 1991.

[17] E. Gnani, A. Gnudi, S. Reggiani, and G. Baccarani, IEEE Trans. Electron Devices, **58**(9), 2903 (2011). https://doi.org/10.1109/TED.2011.2159608.

[18] Abdullayev, J. Sh., & Sapaev, I. B. (2024). Optimization of The Influence of Temperature on The Electrical Distribution of Structures with Radial p-n Junction Structures. East European Journal of Physics, (3), 344-349. https://doi.org/10.26565/2312-4334-2024-3-39.

[19] Тоқтарбайұлы О., Байсариев М., Қайша А., Дуйсебаев Т., Ибраев N., Сериков Т., Ибраимов М., Ханиев В., Тезекбай Y., Жамбыл А., Нураже N., & Сугурбекова G. (2024). Повышение эффективности преобразования энергии в солнечных элементах, чувствительных к красителям, за счет использования полупроводникового материала GaN, синтезированного в печи химического осаждения из газовой фазы с горячими стенками. Eurasian Physical Technical Journal, 21(4(50), 131–139. https://doi.org/10.31489/2024No4/131-139.

[20] Isaev, M.Sh., Khudayberdieva, A.I., Mamatkulov, M.N., Asatov, U.T., Kodirov, S.R. THE SURFACE LAYER MORPHOLOGY OF Si<Cr> SAMPLES, East European Journal of Physics, 2024, 2024(4), pp. 297–300, (https://doi.org/10.26565/2312-4334-2024-4-32).

[21] Olimov, L., Anarboyev, I., Some Electrophysical Properties of Polycrystalline Silicon Obtained in a Solar Oven. Silicon 14, 3817–3822 (2022). (https://doi.org/10.1007/s12633-021-01596-1).

[22] Olimov , L., Anarboyev, I., Mechanism of thermoelectric material efficiency increase, AIP Conf. Proc. 3244, 060015 (2024), (https://doi.org/10.1063/5.0242092).

[23] I. Sapaev, I.B. Sapaev, et. al., E3S Web Conf., 383 (2023) 04022, (https://doi.org/10.1051/e3sconf/202338304022).

[24] Mamadalimov, A.T., Isaev, M.Sh., Mamatkulov, M.N., Kodirov, S.R., Abdurazzokov, STUDY OF SILICIDE FORMATION IN LARGE DIAMETER MONOCRYSTALLINE SILICON, J.T. East European Journal of Physics, 2024, 2024(2), pp. 366–371, (https://doi.org/10.26565/2312-4334-2024-2-45).

[25] Isaev, M.S., Asatov, U.T., Tulametov, M.A., Kodirov, S.R., Rajabov, A.E., STUDY OF THE INHOMOGENEITIES OF OVERCOMPENSED SILICON SAMPLES DOPED WITH MANGANESE, East European Journal of Physics, 2024, 2024(2), pp. 341–344, (https://doi.org/10.26565/2312-4334-2024-2-40).